

Ultrafast vibrations of NaK molecules studied by transient x-ray absorption spectroscopy

Xinran Ren(任欣然), Huihui Wang(王慧慧), Yonggang Yang(杨勇刚)
Citation: Chin. Phys. B. 35, 093101 (2026). DOI: 10.1088/1674-1056/ae48c4 | CSTR: 32038.14.CPB.ae48c4
http://cpb.iphy.ac.cn; http://iopscience.iop.org/cpb

What follows is a list of articles you may be interested in

Theoretical study of the light-induced conical intersection in the photodissociation of molecule OH

Jinqian Liu(刘金倩), Jialong Li(李嘉隆), Dongdong Zhang(张栋栋), Dajun Ding(丁大军)
Chin. Phys. B. 34, 103101 (2025). DOI: 10.1088/1674-1056/addcbb | CSTR: 32038.14.CPB.addcbb

Zero-point fluctuation of hydrogen bond in water dimer from ab initio molecular dynamics

Wan-Run Jiang(姜万润), Rui Wang(王瑞), Xue-Guang Ren(任雪光), Zhi-Yuan Zhang(张志远), Dan-Hui Li(李丹慧), Zhi-Gang Wang(王志刚)
Chin. Phys. B. 29, 103101 (2020). DOI: 10.1088/1674-1056/abab6d

Mechanism analysis of reaction S+(^{2}D)+H_2($X^1\Sigma g+$)→SH+($X^3\Sigma-$)+H(^{2}S) based on the quantum state-to-state dynamics

Jin-Yu Zhang(张金玉), Ting Xu(许婷), Zhi-Wei Ge(葛志伟), Juan Zhao(赵娟), Shou-Bao Gao(高守宝), Qing-Tian Meng(孟庆田)
Chin. Phys. B. 29, 063101 (2020). DOI: 10.1088/1674-1056/ab889c

Study of highly excited vibrational dynamics of HCP integrable system with dynamic potential methods

Aixing Wang(王爱星), Lifeng Sun(孙立风), Chao Fang(房超), Yibao Liu(刘义保)
Chin. Phys. B. 29, 013101 (2020). DOI: 10.1088/1674-1056/ab593a

State-to-state dynamics of F(^{2}P)+HO($^2\Pi$) →O(^{3}P)+HF($^1\Sigma+$) reaction on 1^3A" potential energy surface

Juan Zhao(赵娟), Hui Wu(吴慧), Hai-Bo Sun(孙海波), Li-Fei Wang(王立飞)
Chin. Phys. B. 27, 023102 (2018). DOI: 10.1088/1674-1056/27/2/023102

Ultrafast vibrations of NaK molecules studied by transient x-ray absorption spectroscopy

Xinran Ren(任欣然)[1], Huihui Wang(王慧慧)[1,†], and Yonggang Yang(杨勇刚)[1,2,‡]

[1] *State Key Laboratory of Quantum Optics Technologies and Devices, Institute of Laser Spectroscopy, Shanxi University, Taiyuan* 030006, *China*

[2] *Collaborative Innovation Center of Extreme Optics, Shanxi University, Taiyuan* 030006, *China*

(Received 26 December 2025; revised manuscript received 5 February 2026; accepted manuscript online 23 February 2026)

Time-resolved x-ray absorption spectroscopy is a widely used technique for monitoring ultrafast dynamics of molecules. Here we use this technique to analyze the quantum nuclear dynamics of NaK molecules in the first excited state. To quantitatively reconstruct the vibrational dynamics, we introduce a similarity function to determine the time-dependent position of the nuclear wavepacket from the time-resolved x-ray absorption spectroscopy. Here we demonstrate this new approach through numerical simulations.

Keywords: vibrational dynamics, time-resolved x-ray absorption spectrum, nuclear wavepacket

PACS: 31.10.+z, 78.70.Dm, 82.53.–k

DOI: 10.1088/1674-1056/ae48c4 **CSTR:** 32038.14.CPB.ae48c4

1. Introduction

Molecular spectroscopy is an important tool to investigate molecular structures and properties in detail.[1–3] The integration of molecular spectroscopy with ultrafast time-resolved techniques enables real-time analysis of nanoscale dynamics, offering unprecedented insights into transient species evolution and energy transfer pathways on femtosecond-to-nanosecond timescales. This approach has proven particularly valuable in the study of transition metal complexes[4–7] with a focus on excited-state relaxation dynamics in complex systems. For example, picosecond x-ray absorption spectroscopy can track the structural relaxation of $[Ru^{II}(bpy)_3]^{2+}$ from a high-spin to low-spin state, a process driven by metal-to-ligand charge transfer.[5]

Time-resolved x-ray absorption spectroscopy (TRXAS) has become a powerful tool for monitoring molecular dynamics in real time. Its applications span a wide range of fields, including chemical reactions,[8,9] catalysis,[10] energy conversion,[11] and materials science.[12] TRXAS sheds light on reaction mechanisms by examining intermediate formation, reaction pathways, and dissociative ionization,[8] while also contributing to catalyst design. In Ref. [8], photo-induced chemical reactions in the lowest electronic states of isolated CF_4^+ and SF_6^+ molecules were investigated using TRXAS to characterize the reaction paths and explore the effects of symmetry breaking and Rydberg-valence mixing.

Rapid advancements in x-ray sources, including large-scale x-ray free-electron lasers (XFELs)[13–17] and laboratory-based high-harmonic generation (HHG) setups,[8,18–20] have made it possible to achieve femtosecond or even shorter temporal resolution. These innovations have sparked TRXAS experiments that capture ultrafast dynamics, ranging from ionization,[21,22] excitation,[19] bond breaking,[23] to molecular vibrations.[24,25] In addition, theoretical simulations play a crucial and challenging role in interpreting these complex dynamics[26–28] and analyzing experimental signals. Combined experimental and theoretical investigations have been performed to reveal ultrafast relaxation processes following ionization using attosecond transient absorption spectroscopy.[21,22,24] Typical applications include direct observation of sub-7-femtosecond electronic relaxation in ethylene cation mediated by conical intersection[24] as well as successful detection and analysis of femtosecond symmetry breaking and coherence relaxation in methane cations.[21] Recently, real-time observation of electron dynamics following valence ionization in liquid water, utilizing paired attosecond x-ray pulses, was reported in Ref. [22]. These studies open new avenues for exploring complex systems at their natural time scales.

Apart from illustrating electronic structure dynamics, TRXAS is also widely used to unravel the nuclear dynamics of molecules.[25,29–36] It has the potential to resolve competing channels in excited-state non-adiabatic dynamics[36] and provide insights into core-excited potential energy surfaces by monitoring core-level excitation energy changes with x-ray probes after exciting vibrational superpositions.[25] Information on the vibrational dynamics of molecules is typically obtained indirectly by comparing experimentally

†Corresponding author. E-mail: huihuiwang2019@sxu.edu.cn

‡Corresponding author. E-mail: ygyang@sxu.edu.cn

© 2026 Chinese Physical Society and IOP Publishing Ltd. All rights, including for text and data mining, AI training, and similar technologies, are reserved.

measured differential absorption spectra with theoretical calculations.[25,29,31,33–35] Notable examples include utilizing the sensitivity of 3d core-level transient absorption spectroscopy to bond length and charge state to investigate the evolution of the ground and ionized state vibrational wavepackets produced by strong-field ionization of Br_2,[29] and explaining the oscillation in the 1s-2π peak energy of the electronic ground state of NO^+, triggered by strong-field ionization, through potential energy curves of NO and NO^+ obtained from ab initio calculations.[31]

From the theoretical point of view, it is possible to calculate the TRXAS using information from the time-dependent nuclear wavepacket. However, the inverse reconstruction of the corresponding nuclear wavepacket from the TRXAS data remains a challenging task. In this work, we report the inverse reconstruction of the nuclear wavepacket position for the NaK molecule from its TRXAS. The theoretical framework underlying this work is detailed in Section 2. The results and the discussion are in Section 3. The conclusions are in Section 4.

2. Theory and model

The time-dependent molecular wavefunction $\Psi(\boldsymbol{r},R,t)$ can be expressed by the Born–Huang expansion

$$\Psi(\boldsymbol{r},R,t)=\sum_{\alpha}\chi_{\alpha}(R,t)\phi_{\alpha}(\boldsymbol{r},R), \tag{1}$$

where $\boldsymbol{r}$ and R denote the electronic and the nuclear coordinates, respectively. The wavefunction $\phi(\boldsymbol{r},R)$ of the electronic state $|\alpha\rangle$ can be obtained by solving the electronic Schrödinger equation

$$H_{\rm el}\phi_{\alpha}(\boldsymbol{r},R)=V_{\alpha}(R)\phi_{\alpha}(\boldsymbol{r},R), \tag{2}$$

where $H_{\rm el}$ is the electronic Hamiltonian and $V_{\alpha}(R)$ is the potential energy curve of state $|\alpha\rangle$. The electronic Hamiltonian $H_{\rm el}$ can be expressed as

$$H_{\rm el}=T_{\rm el}+V_{\rm el-el}+V_{\rm el-nuc}+V_{\rm nuc-nuc}+V_{\rm so}, \tag{3}$$

where $T_{\rm el}=-\frac{\hbar^2}{2m_{\rm e}}\sum_i\nabla_i^2$ is the electronic kinetic energy operator with ∇_i^2 being the Laplacian operator of the i-th electron; $V_{\rm el-el}=\sum_{i<j}\frac{e^2}{4\pi\varepsilon_0 r_{ij}}$ is the potential energy of electron–electron interactions with r_{ij} being the distance between the i-th and j-th electrons; $V_{\rm el-nuc}=-\sum_{i,A}\frac{Z_A e^2}{4\pi\varepsilon_0 r_{iA}}$ is the potential energy of electron–nuclear interactions with Z_A and r_{iA} being the nuclear charge of nucleus A and the distance between the i-th electron and nucleus A; $V_{\rm nuc-nuc}=\sum_{A<B}\frac{Z_A Z_B e^2}{4\pi\varepsilon_0 r_{AB}}$ is the potential energy of nuclear–nuclear interactions with r_{AB} being the distance between nucleus A and nucleus B. The last term $V_{\rm so}$ includes spin–orbit coupling. The spin–orbit coupling is calculated using the Breit–Pauli operator.[37] Relativistic effects are included by the Douglas–Kroll–Hess (DKH) Hamiltonian as implemented in MOLPRO.[38]

The ground state of the system is $\chi_{g0}(R)\phi_g(\boldsymbol{r},R)$, where $\chi_{g0}(R)$ is the vibrational ground state wavefunction of the electronic ground state $|g\rangle$. It is obtained by the diagonalization of the matrix form for the nuclear Hamiltonian $H_{\rm nuc}=T_{\rm nuc}+V_g(R)=-\frac{\hbar^2}{2\mu}\frac{\partial^2}{\partial R^2}+V_g(R)$ with $\mu=\frac{m_{\rm Na}m_{\rm K}}{m_{\rm Na}+m_{\rm K}}$. The matrix form is obtained by the Fourier grid Hamiltonian.[39]

The system can be prepared in the first electronic excited state $|e\rangle$ characterized by the initial wavefunction

$$\Psi(\boldsymbol{r},R,t=0)\approx\chi_e(R,t=0)\phi_e(\boldsymbol{r},R), \tag{4}$$

where $\chi_e(R,t=0)\approx\chi_{g0}(R)$ for typical ultrafast laser excitations. Subsequently, the system propagates according to the time-dependent Schrödinger equation

$$\begin{aligned}\mathrm{i}\hbar\frac{\partial}{\partial t}\chi_{\alpha}(R,t) &= (T_{\rm nuc}+V_{\alpha}(R))\chi_{\alpha}(R,t)\\ &\quad+\sum_{\beta}H_{\alpha\beta}(R)\chi_{\beta}(R,t),\end{aligned} \tag{5}$$

where $H_{\alpha\beta}(R)$ represents the nonadiabatic couplings. Each block of the Hamiltonian matrix, namely each of the nuclear operators $T_{\rm nuc}+V_{\alpha}(R)$ and $H_{\alpha\beta}(R)$, is generated by the Fourier grid Hamiltonian[39] to form the entire vibronic Hamiltonian matrix. Equation (5) is then propagated by means of the Crank–Nicolson method.[40]

The nonadiabatic couplings $H_{\alpha\beta}(R)$ are directly calculated numerically. The numerical solution of Eq. (5) reveals that the nonadiabatic transitions from the first excited state $|e\rangle$ to the other electronic states are negligible. Accordingly, the time-dependent wavefunction can be approximated as

$$\Psi(\boldsymbol{r},R,t)\approx\chi_e(R,t)\phi_e(\boldsymbol{r},R). \tag{6}$$

To calculate the TRXAS, we first obtain the x-ray absorption cross section according to Fermi's golden rule, as described in Refs. [8,9]

$$\sigma(\omega,R)=\frac{4\pi^2\omega}{3c}\sum_{\alpha}|\mu_{e\alpha}(R)|^2\delta[V_{\alpha}(R)-V_e(R)-\hbar\omega], \tag{7}$$

where $\mu_{e\alpha}(R)$ is the transition dipole moment between the electronic states $|e\rangle$ and $|\alpha\rangle$. In our numerical calculations, the delta function in Eq. (7) is replaced by a Gaussian function $\frac{1}{\sqrt{\pi\hbar\Gamma}}e^{-[\omega-\frac{V_{\alpha}(R)-V_e(R)}{\hbar}]^2/\Gamma^2}$ with a phenomenological width parameter $\hbar\Gamma=0.05$ eV. The TRXAS $\sigma(\omega,t)$ is calculated by an incoherent weighting of Eq. (7) as

$$\sigma(\omega,t)=\int\sigma(\omega,R)|\chi_e(R,t)|^2\,\mathrm{d}R. \tag{8}$$

All the quantum chemistry calculations are performed at the CASSCF/cc-pwCVQZ-DK level of theory using MOLPRO.[38] The required potential energy curves $V_{\alpha}(R)$ and dipole moment curves $\mu_{e\alpha}(R)$ for all the involved electronic states are calculated over the range of nuclear distance R from 2.00 Å to 6.50 Å, with the step size 0.01 Å.

3. Results and discussion

3.1. The stationary x-ray absorption spectrum of NaK

The calculated equilibrium bond length of NaK is 3.49 Å, which is consistent with Refs. [41,42]. The main electronic configuration of the ground state $|g\rangle$ is $1\sigma^2 2\sigma^2 3\sigma^2 4\sigma^2 1\pi^4 5\sigma^2 6\sigma^2 7\sigma^2 2\pi^4 8\sigma^2 3\pi^4 9\sigma^2$. This will be shortened as $2\sigma^2 9\sigma^2$ in the subsequent context. The active space for CASSCF calculations contains two occupied orbitals 2σ, 9σ and 22 virtual orbitals up to 19σ, 8π, 2δ. The first excited state $|e\rangle$ has the main electronic configuration $2\sigma^2 9\sigma^1 10\sigma^1$. Here the molecular orbital 2σ is the 1s orbital of the sodium atom. Both the states $|g\rangle$ and $|e\rangle$ belong to the symmetry $\Omega = 0^+$. Rigorous notations for these two states are $(1)0^+$ and $(2)0^+$, respectively. According to the calculations, both $|g\rangle$ and $|e\rangle$ are contributed by more than 99% $^1\Sigma^+$ and less than 1% $^3\Pi$ states. Therefore we simply use the notations $X^1\Sigma^+$ and $A^1\Sigma^+$ for the states $|g\rangle$ and $|e\rangle$, respectively.

We consider the five lowest excited states, which involve the excitation of one electron from the 1s orbital of the Na atom. This means the sodium K-edge absorption spectroscopy. The corresponding spectrum calculated at the equilibrium structure of the NaK molecule is presented in Fig. 1. This spectrum spans an energy range from 1092.5 eV to 1095.5 eV and features five distinct peaks. Each peak primarily originates from a two-electron transition: one electron is transferred from the 10σ orbital to the 9σ orbital, while another electron is excited from the 2σ orbital to a higher molecular orbital. To simplify notation, we will omit the explicit reference to the common transition from 10σ to 9σ for all five peaks, representing each peak instead by a single transition from the 2σ orbital.

The peaks at 1092.80 eV, 1093.97 eV and 1094.80 eV are assigned to the transitions $2\sigma \to 10\sigma$, $2\sigma \to 11\sigma$ and $2\sigma \to 12\sigma$, respectively. Namely, the main electronic configurations of the corresponding transition final states are $2\sigma^1 9\sigma^2 10\sigma^1$, $2\sigma^1 9\sigma^2 11\sigma^1$ and $2\sigma^1 9\sigma^2 12\sigma^1$, respectively. The three σ orbitals 10σ, 11σ and 12σ are mainly contributed by the s and p_z orbitals of Na and K atoms. Here z denotes the direction along the molecular axis. The weights of the p_z orbitals of Na atom decrease from 10σ to 12σ when the orbital energy increases. Accordingly, the intensities of these three peaks decrease when the excitation energy increases.

The absorption features observed at 1093.5 eV and 1094.77 eV are attributed to transitions from the 2σ orbital to the 4π and 5π orbitals, respectively. These two π orbitals are predominantly formed by the p_x (or p_y) orbitals of the Na and K atoms. The key difference between them is that the contribution of the Na atomic orbitals is much larger in the 4π orbital than in the 5π orbital. The dominant contribution of Na atomic p orbitals to the molecular 4π orbital leads to the most intense $2\sigma \to 4\pi$ transition within the energy range shown in Fig. 1. For more details, color contour plots of these six molecular orbitals are provided in the bottom panel of Fig. 1.

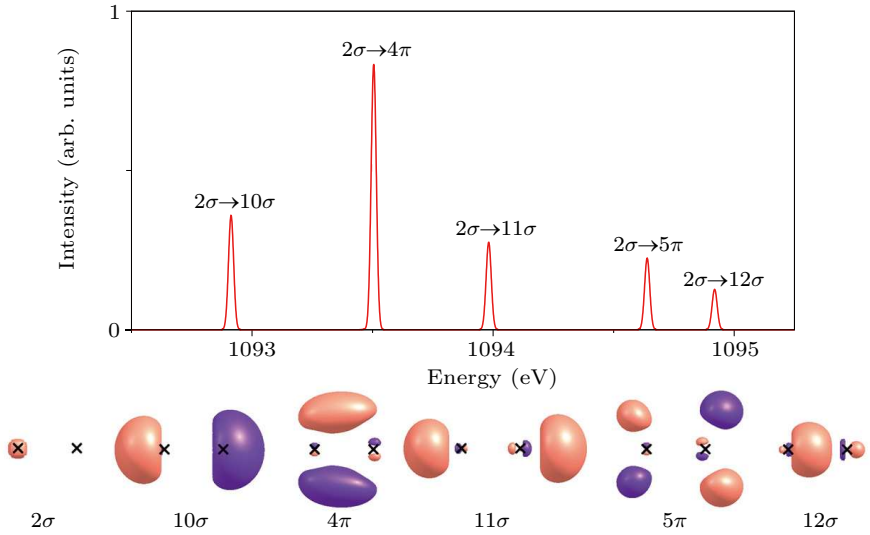


Fig. 1. The sodium K-edge x-ray absorption spectrum of NaK at the equilibrium structure. The six involved molecular orbitals are shown in the bottom panel. Two "×" symbols are added to each orbital to indicate the positions of the Na (left) and K (right) atoms.

3.2. The time-resolved x-ray absorption spectrum and vibrational dynamics of NaK

The initial wavepacket of NaK, expressed in Eq. (4) and shown as a blue curve in Fig. 3(a), is populated in the first excited state $A^1\Sigma^+$ following ultrafast vertical excitation from the electronic ground state. After excitation, the wavepacket propagates freely until the transient x-ray absorption spectrum is recorded at a later time t. The possibility of nonadiabatic transitions from the initial $A^1\Sigma^+$ state to nearby electronic states is taken into account. Each of these nearby states is predominantly characterized by one of the following: $^1\Sigma^+$, $^3\Sigma^+$, $^1\Pi$, or $^3\Pi$, with a contribution greater than 99%. The nona-

diabatic coupling matrix elements between the $^1\Sigma^+$ states and the $^3\Sigma^+$ (or $^1\Pi$, $^3\Pi$) states are zero for NaK. We specifically focus on calculating the nonadiabatic transitions between the three lowest $^1\Sigma^+$ states. The transitions from the $A^1\Sigma^+$ state to the other two nearby $^1\Sigma^+$ states contribute less than 1%. Subsequently, we focus on the vibrational dynamics of NaK in the $A^1\Sigma^+$ state. Accordingly, the wavepacket travels from the equilibrium structure at $R = 3.5$ Å to the right turning point at $R = 5.2$ Å in approximately 234 fs, then returns to the left turning point at around $t \approx 468$ fs. The detailed dynamics of this wavepacket are shown in Fig. 3(b), where two horizontal lines are used to indicate the times when the wavepacket reaches the left and right turning points.

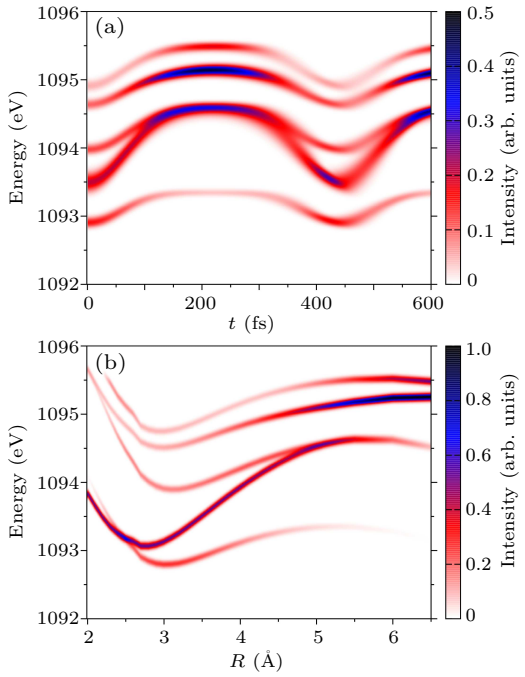


Fig. 2. (a) Time-resolved x-ray absorption spectrum $\sigma(\omega,t)$ for $t \leq 600$ fs. (b) The x-ray absorption cross section $\sigma(\omega,R)$ for different molecular structures.

Using the time-dependent nuclear wavefunction, the TRXAS $\sigma(\omega,t)$ is calculated according to Eq. (8). The resulting spectrum is shown in Fig. 2(a), which reflects the real-time nuclear dynamics of NaK in the $A^1\Sigma^+$ state. The spectrum exhibits oscillations with a period of approximately 460 fs, corresponding to the nuclear wavepacket dynamics shown in Fig. 3(b). At $t = 0$ fs, five absorption bands appear at 1092.8 eV, 1093.5 eV, 1094.0 eV, 1094.6 eV, and 1094.9 eV. For the first half of the oscillatory period, the transition energies of these bands increase with time. Notably, the absorption signals initially located at 1093.5 eV and 1093.97 eV overlap and merge at 1094.0 eV, forming a pronounced absorption feature. This feature persists for approximately 200 fs before the absorption signals separate again. During the first half of the vibrational period, as the nuclear wavepacket propagates from its initial position to the right turning point, the intensity of the lowest absorption band decreases while the intensities of the other four bands increase. The extremal intensities for all five bands are reached when the wavepacket reaches the right turning point. The second half period is roughly a mirror image of the first half. The stationary x-ray absorption cross section $\sigma(\omega,R)$, as a function of internuclear distance R, serves as the fundamental input for both the theoretical calculations of TRXAS $\sigma(\omega,t)$ and the inverse quantitative analysis of nuclear dynamics from the TRXAS data. Figure 2(b) displays the $\sigma(\omega,R)$ at different values of R, as described by Eq. (7). It is evident that $\sigma(\omega,R)$ is sensitive to the geometry structure, indicating that the dominant transition characteristics vary with molecular geometry. At the equilibrium position ($R = 3.5$ Å), transitions from the 2σ molecular orbital to the other five orbitals contribute to the spectrum. Notably, the transition to the 4π orbital has a significantly larger intensity than the transitions to the other orbitals, as shown in both Figs. 2(b) and 1. In contrast, when the internuclear distance R exceeds 5.0 Å, the transition from the 2σ orbital to the 5π orbital becomes dominant. Furthermore, the peak for the transition $2\sigma \rightarrow 10\sigma$ disappears when the internuclear distance R exceeds 5.5 Å. This is because, as the internuclear distance R increases, the weights of the p_z orbitals of the Na atom in the 10σ and 11σ orbital decreases, while the weight in the 12σ orbital increases. As the internuclear distance R further increases into the dissociation region, the molecular orbitals gradually change to atomic orbitals. Specifically, the 9σ and 10σ orbitals become the s orbitals of Na and K atoms, respectively. In this region, all the $\sigma(\omega,R)$ intensities for $R > 10$ Å in the energy window of Fig. 2(b) become zero due to the forbidden transition from 10σ to 9σ. For the present work, only the data of $\sigma(\omega,R)$ for $R < 6$ Å are required.

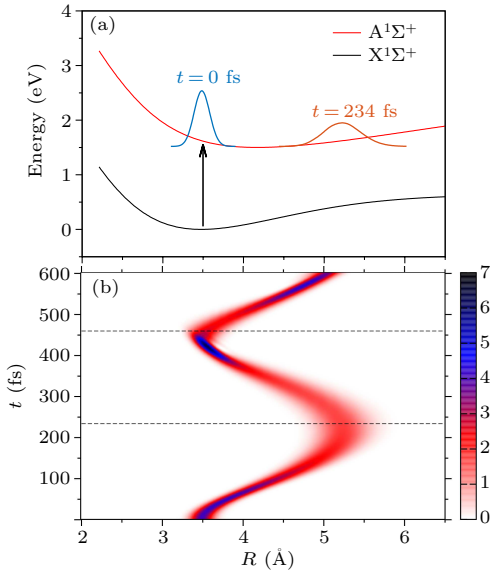


Fig. 3. (a) The potential energy curves of NaK for the $X^1\Sigma^+$ and $A^1\Sigma^+$ states. The initial wavepacket (blue) in the first electronic excited state propagates to the right turning point at about $t = 234$ fs, see the purple curve. (b) Propagation of the wavepacket for $t \leq 600$ fs.

To quantitatively analyze molecular vibrational dynamics from TRXAS $\sigma(\omega,t)$, the ultimate goal is to reconstruct the time-dependent nuclear wavepacket. The most intuitive and straightforward approach, however, involves examining the expectation value $\langle R\rangle$ of the nuclear wavepacket. This offers a direct way to illustrate the vibrational dynamics. To determine the position of the nuclear wavepacket $R(t)$ at a given time t, we need to analyze the spectrum $\sigma(\omega,t)$ at this specific time. This requires comparing the spectrum $\sigma(\omega,t)$ at a given time t with the cross-section $\sigma(\omega,R)$ at different nuclear distances. If the spectrum at a given time t closely matches the cross-section for a specific internuclear distance R, we can conclude that at this particular time t, the nuclear wavepacket reaches this specific nuclear distance R.

The key task is therefore to quantitatively compare the TRXAS $\sigma(\omega,t)$ with the cross section $\sigma(\omega,R)$. For this purpose, we define the following similarity function:

$$S(R,t)=\frac{\int\sigma(\omega,t)\sigma(\omega,R)\,\mathrm{d}\omega}{\sqrt{\int\sigma(\omega,t)^2\,\mathrm{d}\omega}\sqrt{\int\sigma(\omega,R)^2\,\mathrm{d}\omega}} \tag{9}$$

to characterize the similarity between $\sigma(\omega,t)$ and $\sigma(\omega,R)$, for a given t and R. The value of $S(R,t)$ is in the region $0\le S(R,t)\le 1$. If $\sigma(\omega,t=t_0)$ and $\sigma(\omega,R=R_0)$ represent the same spectrum $\sigma(\omega)$, the value of $S(R=R_0,t=t_0)$ will be one. Conversely, if $\sigma(\omega,t)$ and $\sigma(\omega,R)$ have nothing in common, the value of $S(R,t)$ will be zero. A larger value of $S(R,t)$ indicates a higher similarity between $\sigma(\omega,t)$ at t and $\sigma(\omega,R)$ at R. Accordingly, we define the position $R(t)$ of the wavepacket at a given time t as the value of R that maximizes the value of $S(R,t)$. In other words, $R(t)$ corresponds to the root(s) of the following equation:

$$\frac{\partial S(R,t)}{\partial R}=0. \tag{10}$$

This equation is solved numerically to find the maximum of $S(R,t)$ at any given time t and the corresponding value of R, which is the position $R(t)$ of the nuclear wavepacket.

This comparative analysis enables the extraction of the time-dependent position $R(t)$ of the nuclear wavepacket from the time-resolved spectra $\sigma(\omega,t)$. By analyzing these spectra at different time intervals, the evolution of the nuclear wavepacket can be tracked, offering a precise reconstruction of its trajectory over time. This approach provides a robust framework for studying molecular vibrational dynamics and monitoring the motion of the nuclear wavepacket throughout its evolution.

In this way, we reconstruct the time-dependent position $R(t)$ of the nuclear wavepacket for $0\le t\le 600$ fs. The corresponding results are shown in Fig. 4. We further compare $R(t)$ with the quantum mechanical mean value $\langle R\rangle$ of the internuclear distance R in Fig. 4. As can be seen, the agreement is quite good, indicating that the position of the nuclear wavepacket can be quantitatively reconstructed from the TRXAS data.

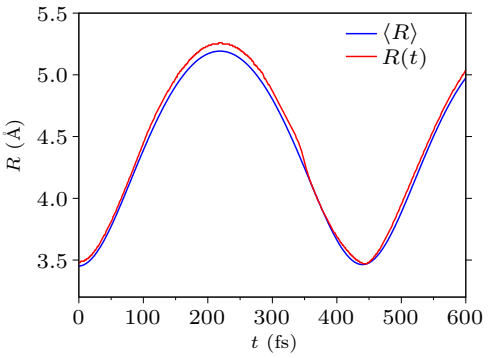


Fig. 4. Time-dependent position $R(t)$ of the nuclear wavepacket of Fig. 3(b) reconstructed from the time-resolved x-ray absorption spectrum $\sigma(\omega,t)$. Also shown is the quantum mechanical mean value $\langle R\rangle$ directly calculated from the nuclear wavepacket of Fig. 3(b) for comparison.

4. Conclusions

In summary, we present a novel theoretical approach for the inverse reconstruction of the time-dependent nuclear wavepacket from TRXAS. This method is successfully applied to investigate the vibrational dynamics of NaK. We define a similarity function that quantitatively compares the TRXAS with x-ray absorption cross-sections of various molecular structures to reconstruct the time-dependent position of the nuclear wavepacket. This reconstruction demonstrates good agreement with the corresponding quantum mechanical mean value obtained by nuclear quantum dynamics simulations, validating the effectiveness of the proposed approach.

This study opens new avenues for quantitative investigations of molecular vibrational dynamics using x-ray techniques. It reveals the relationship between electronic structure and ultrafast vibrational dynamics, thereby advancing the broad field of molecular dynamics research. Our approach can be applied easily to other molecular systems, providing a powerful tool for ultrafast science and molecular quantum control.

However, it is important to acknowledge the scope and limitations of this method. The successful application demonstrated here relies on the fact that the TRXAS of the NaK system exhibits five distinct and well-separated absorption peaks whose energies and intensities vary significantly with the internuclear distance R. This "spectral richness" allows the similarity function $S(R,t)$ to identify a unique maximum at each time step. In contrast, for some molecular systems, the core-level absorption spectrum might consist of only a single broad peak, or the spectral shape might be very similar over a wide range of nuclear geometries. In such cases, the similarity function might yield multiple equivalent maxima for different R values at a given time t, or fail to identify a clear global maximum. Therefore, the similarity-based inversion is expected to be ro-

bust primarily for systems where spectral features are rich and sensitive to geometry changes.

Acknowledgements

We would like to express our gratitude to Prof. Jörn Manz (Freie Universität Berlin) for stimulating discussions. This work was supported in part by the National Natural Science Foundation of China (Grant Nos. 12374267, 12574375, U22A2091, and 11904215), the Program of Changjiang Scholars and Innovative Research Team in University of Ministry of Education of China (Grant No. IRT_17R70), and the Fundamental Research Program of Shanxi Province (Grant No. 202503021211059).

References

[1] Hess Jr B A, Schaad L J, Carsky P and Zahradnik R 1986 *Chem. Rev.* **86** 709
[2] Quillard S, Louarn G, Lefrant S and Macdiarmid A G 1994 *Phys. Rev. B* **50** 12496
[3] Stipe B C, Rezaei M A and Ho W 1998 *Science* **280** 1732
[4] Chen L X, Jäger W H J, Jennings G, Gosztola D J, Munkholm A and Hessler J P 2001 *Science* **292** 262
[5] Saes M, Bressler C, Abela R, Grolimund D, Johnson S L, Heimann P A and Chergui M 2003 *Phys. Rev. Lett.* **90** 047403
[6] Gawelda W, Pham V T, Benfatto M, *et al.* 2007 *Phys. Rev. Lett.* **98** 057401
[7] Kochetov V and Bokarev S I 2022 *J. Chem. Theory Comput.* **18** 46
[8] Pertot Y, Schmidt C, Matthews M, *et al.* 2017 *Science* **355** 264
[9] Loh Z H, Doumy G, Arnold C, *et al.* 2020 *Science* **367** 179
[10] Lin S C, Chang C C, Chiu S Y, Pai H T, Liao T Y, Hsu C S, Chiang W H, Tsai M K and Chen H M 2020 *Nat. Commun.* **11** 3525
[11] Sato T, Nozawa S, Ichiyanagi K, Tomita A, Chollet M, Ichikawa H, Fujii H, Adachi S I and Koshihara S Y 2009 *J. Synchrotron Radiat.* **16** 110
[12] Kooi S E, Leskiw B D and Castleman A W 2001 *Nano Lett.* **1** 113
[13] Bressler Ch, Milne C, Pham V T, *et al.* 2009 *Science* **323** 489
[14] Lemke H T, Bressler C, Chen L X, *et al.* 2013 *J. Phys. Chem. A* **117** 735
[15] Ogi Y, Obara Y, Katayama T, *et al.* 2015 *Struct. Dyn.* **2** 034901
[16] Levantino M, Lemke H T, Schirò G, Glownia M, Cupane A and Cammarata M 2015 *Struct. Dyn.* **2** 041713
[17] Shelby M L, Lestrange P J, Jackson N E, *et al.* 2016 *J. Am. Chem. Soc.* **138** 8752
[18] Loh Z H, Khalil M, Correa R E, Santra R, Buth C and Leone S R 2007 *Phys. Rev. Lett.* **98** 143601
[19] Attar A R, Bhattacherjee A, Pemmaraju C D, Schnorr K, Closser K D, Prendergast D and Leone S R 2017 *Science* **356** 54
[20] Smith A D, Balčiūnas T, Chang Y P, *et al.* 2020 *J. Phys. Chem. Lett.* **11** 1981
[21] Ridente E, Hait D, Haugen E A, Ross A D, Neumark D M, Head-Gordon M and Leone S R 2023 *Science* **380** 713
[22] Li S, Lu L, Bhattacharyya S, *et al.* 2024 *Science* **383** 1118
[23] Loh Z H and Leone S R 2008 *J. Chem. Phys.* **128** 204302
[24] Zinchenko K S, Ardana-Lamas F, Seidu I, Neville S P, van der Veen J, Utrio Lanfaloni V, Schuurman M S and Wörner H J 2021 *Science* **371** 489
[25] Ross A D, Hait D, Scutelnic V, Neumark D M, Head-Gordon M and Leone S R 2024 *Commun. Phys.* **7** 304
[26] Neville S P, Chergui M, Stolow A and Schuurman M S 2018 *Phys. Rev. Lett.* **120** 243001
[27] Shakya Y, Inhester L, Arnold C, Welsch R and Santra R 2021 *Struct. Dyn.* **8** 034102
[28] Segatta F, Aranda D, Aleotti F, Montorsi F, Mukamel S, Garavelli M, Santoro F and Nenov A 2024 *J. Chem. Theory Comput.* **20** 307
[29] Hosler E R and Leone S R 2013 *Phys. Rev. A* **88** 023420
[30] Wei Z, Li J, Wang L, See S T, Jhon M H, Zhang Y, Shi F, Yang M and Loh Z H 2017 *Nat. Commun.* **8** 735
[31] Saito N, Sannohe H, Ishii N, Kanai T, Kosugi N, Wu Y, Chew A, Han S, Chang Z and Itatani J 2019 *Optica* **6** 1542
[32] Timmers H, Zhu X, Li Z, Kobayashi Y, Sabbar M, Hollstein M, Reduzzi M, Martínez T J, Neumark D M and Leone S R 2019 *Nat. Commun.* **10** 3133
[33] Kobayashi Y, Chang K F, Zeng T, Neumark D M and Leone S R 2019 *Science* **365** 79
[34] Kobayashi Y, Chang K F, Poullain S M, Scutelnic V, Zeng T, Neumark D M and Leone S R 2020 *Phys. Rev. A* **101** 063414
[35] Garratt D, Misiekis L, Wood D, *et al.* 2022 *Nat. Commun.* **13** 3414
[36] Seidu I, Neville S P, MacDonell R J and Schuurman M S 2022 *Phys. Chem. Chem. Phys.* **24** 1345
[37] Heß B A, Marian C M, Wahlgren U and Gropen O 1996 *Chem. Phys. Lett.* **251** 365
[38] Werner H J, Knowles P J, Knizia G, *et al.* 2012 *Molpro* **2012.1** (see http://www.molpro.net)
[39] Marston C C and Balint-Kurti G G 1989 *J. Chem. Phys.* **91** 3571
[40] Crank J and Nicolson P 1947 *Math. Proc. Cambridge Philos. Soc.* **43** 50
[41] Bączek K, Jasik P, Kilich T and Sienkiewicz J E 2022 *Mol. Phys.* **120** e2040628
[42] Chen Y, Haase D, Manz J, Wang H and Yang Y 2024 *Nat. Commun.* **15** 565